


Article

Direct Synthesis of MoS₂ Nanosheets in Reduced Graphene Oxide Nanoscroll for Enhanced Photodetection

Zhikang Wu, Feifei Li, Xiya Li, Yang Yang, Xiao Huang * and Hai Li * 

Key Laboratory of Flexible Electronics (KLOFE) & Institute of Advanced Materials (IAM), Nanjing Tech University (Nanjing Tech), 30 South Puzhu Road, Nanjing 211816, China; iamzkwu@njtech.edu.cn (Z.W.); lifeifei@njtech.edu.cn (F.L.); lixiya@njtech.edu.cn (X.L.); iamyyang@njtech.edu.cn (Y.Y.)

* Correspondence: iamxhuang@njtech.edu.cn (X.H.); iamhli@njtech.edu.cn (H.L.)

Abstract: Due to their unique tubular and spiral structure, graphene and graphene oxide nanoscrolls (GONS) have shown extensive applications in various fields. However, it is still a challenge to improve the optoelectronic application of graphene and GONS because of the zero bandgap of graphene. Herein, ammonium tetrathiomolybdate ((NH₄)₂MoS₄) was firstly wrapped into the ((NH₄)₂MoS₄@GONS) by molecular combing the mixture of (NH₄)₂MoS₄ and GO solution on hydrophobic substrate. After thermal annealing, the (NH₄)₂MoS₄ and GO were converted to MoS₂ nanosheets and reduced GO (RGO) simultaneously, and, thus, the MoS₂@RGONS was obtained. Raman spectroscopy and high-resolution transmission electron microscopy were used to confirm the formation of MoS₂ nanosheets among the RGONS. The amount of MoS₂ wrapped in RGONS increased with the increasing height of GONS, which is confirmed by the atomic force microscopy and Raman spectroscopy. The as-prepared MoS₂@RGONS showed much better photoresponse than the RGONS under visible light. The photocurrent-to-dark current ratios of photodetectors based on MoS₂@RGONS are ~570, 360 and 140 under blue, red and green lasers, respectively, which are 81, 144 and 35 times of the photodetectors based on RGONS. Moreover, the MoS₂@RGONS-based photodetector exhibited good power-dependent photoresponse. Our work indicates that the MoS₂@RGONS is expected to be a promising material in the fields of optoelectronic devices and flexible electronics.

Keywords: ammonium tetrathiomolybdate; thermal annealing; MoS₂@reduced graphene oxide nanoscroll; photosensitivity; photodetection



Citation: Wu, Z.; Li, F.; Li, X.; Yang, Y.; Huang, X.; Li, H. Direct Synthesis of MoS₂ Nanosheets in Reduced Graphene Oxide Nanoscroll for Enhanced Photodetection. *Nanomaterials* **2022**, *12*, 1581. <https://doi.org/10.3390/nano12091581>

Academic Editor: Jun-ho Yum

Received: 15 April 2022

Accepted: 4 May 2022

Published: 6 May 2022

Publisher's Note: MDPI stays neutral with regard to jurisdictional claims in published maps and institutional affiliations.



Copyright: © 2022 by the authors. Licensee MDPI, Basel, Switzerland. This article is an open access article distributed under the terms and conditions of the Creative Commons Attribution (CC BY) license (<https://creativecommons.org/licenses/by/4.0/>).

1. Introduction

By scrolling two-dimensional graphene nanosheet into a one-dimensional structure, a graphene nanoscroll (GNS) is formed with a tubular, spiral structure and open ends [1]. Due to the excellent properties resulting from its unique structure, graphene nanoscroll has attracted great attention in the fields of energy storage, sensors and flexible electronics [2–5]. In recent years, graphene oxide nanoscrolls (GONS) have been widely investigated instead of GNS because of the facile mass production of graphene oxide [2,6–15]. In order to further improve the performance of GONS, various functional nanomaterials were wrapped into GONS to extend their applications in supercapacitors, batteries and photocatalysts [16–20]. By encapsulating sulfur into GONS during the freeze-casting process, the as-prepared S/GONS was used as a good cathode material for a lithium-sulfur battery [21,22]. After Fe₂O₃ nanoparticles were wrapped into GONS as electrode materials by ultrasonication, a high volumetric energy density supercapacitor with quite good cycling stability was obtained [23]. Fe_{1-x}S/Fe₃O₄ nanoparticles were also confined into GONSs and GO nanosheets by cold quenching and freeze drying, and the as-obtained composites were used as promising electrodes for a flexible lithium-ion battery [3].

It is well known that the application of graphene in high-performance photodetectors has been seriously hindered due to its low optical absorption ability [24]. To improve

the photoresponse of graphene-based devices, a large number of functional nanomaterials have been integrated with graphene, including quantum dots [24], transition metal dichalcogenides [25–27], metallic nanostructures with plasmonic effects [28,29] and so on. Although the GONS has shown promising applications in the fields of energy storage, sensing and photocatalysis, it is still a challenge to apply the GONS as a high-performance photodetector. Previously, we have embedded chemical vapor deposition (CVD)-grown MoS₂ nanoflakes into RGO nanoscrolls to improve the photodetection performance [25]. The photosensitivity of MoS₂@RGO nanoscrolls increased by 20 times compared to the RGO nanosheet. However, it is difficult to further increase the amount of MoS₂ grown on an RGO nanosheet by using the CVD method. Therefore, it is highly desirable to develop an alternative method to wrap a large amount of MoS₂ into GONS and thus further enhance its photodetection performance.

In this work, a large amount of a precursor, ammonium tetrathiomolybdate ((NH₄)₂MoS₄), was successfully wrapped into GONSs with length up to hundreds of micrometers by using the molecular combing method. After high temperature annealing, the (NH₄)₂MoS₄ was in situ decomposed to MoS₂ nanosheets, which were well encapsulated into the GONS. Meanwhile, the GONSs were simultaneously converted to reduced GONSs (RGONS). By optimizing precursor concentration and annealing temperature, high-quality MoS₂@RGONS was readily obtained with mass production. The optical microscopy (OM), atomic force microscopy (AFM), high-resolution transmission electron microscopy (HRTEM) and Raman spectroscopy were employed to demonstrate the uniform distribution of MoS₂ nanosheets in RGONSs. The photodetectors based on MoS₂@RGONSs showed photosensitivity two orders of magnitude higher than that of the RGONS under visible light. The MoS₂@RGONSs-based photodetectors also exhibited good power dependent behavior. The improved performance could be attributed to the formation of multiple graphene/MoS₂ interfaces in the scrolled structure of MoS₂@RGONS, which increases the light absorption efficiency and enables the ultrafast charge transfer, resulting in a much higher photocurrent and photosensitivity.

2. Experimental Section

2.1. Preparation of (NH₄)₂MoS₄ Solution and Hydrophobic Substrate

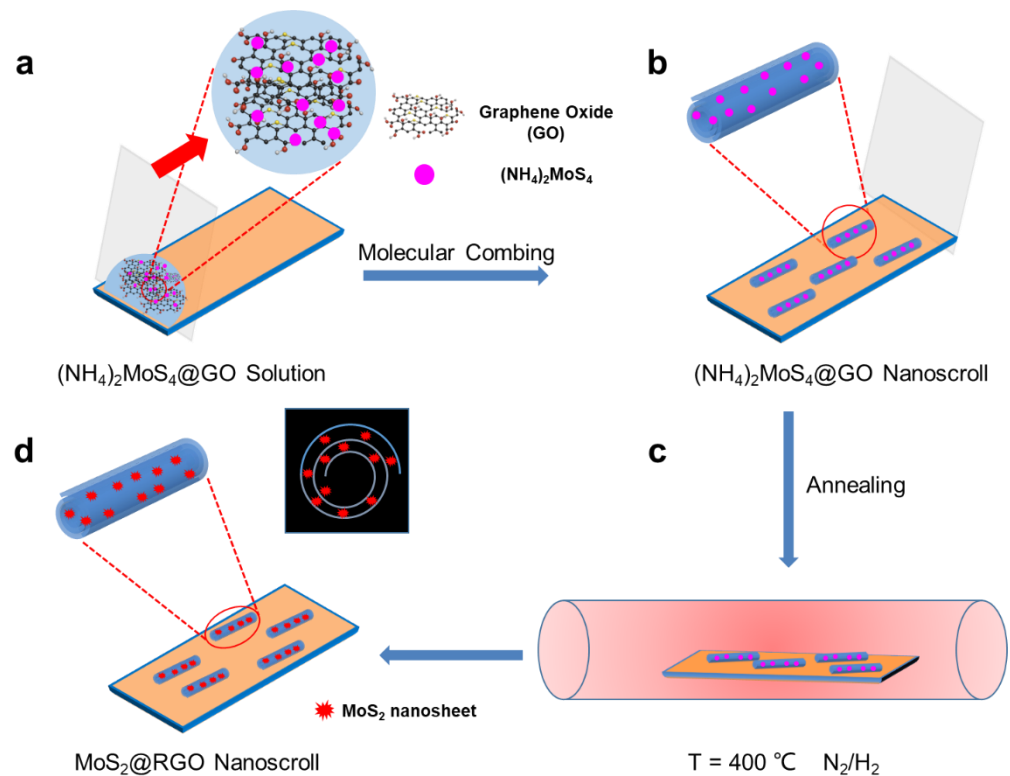
Graphene oxide (GO) was synthesized by the modified Hummers method. A total of 0.038 g of (NH₄)₂MoS₄ was ground to fine powder and dissolved in water to form aqueous solutions with concentration of 5, 10, 20, 30 and 50 mM. Thereafter, the (NH₄)₂MoS₄ solution was treated by ultrasonication to ensure complete dissolution. Finally, the (NH₄)₂MoS₄@GO solution was prepared by mixing 0.2 mg/mL GO and (NH₄)₂MoS₄ solution with a volume ratio of 1:1.

The preparation of hydrophobic substrate is a key step to form GO nanoscrolls by the molecular combing method [6,7,10,11]. Firstly, the cleaned 300 nm SiO₂/Si substrate was immersed into a glass bottle containing a mixture of 8 mL toluene and 200 μL OTS (Octadecyltrimethoxysilane, purchased from Aladdin). Then, the glass bottle was sealed and heated at 60 °C for 24 h. After that, the SiO₂/Si substrate was washed with ethanol and DI water three times. Therefore, the hydrophobic OTS-modified SiO₂/Si substrate (OTS-SiO₂/Si) was obtained.

2.2. Preparation of (NH₄)₂MoS₄@GONS and MoS₂@RGONS

The (NH₄)₂MoS₄@GO nanoscrolls ((NH₄)₂MoS₄@GONSs) were prepared by the molecular combing method [6], as shown in Scheme 1a,b. Firstly, 30 μL of the (NH₄)₂MoS₄@GO solution was dropped onto the hydrophobic OTS-SiO₂/Si substrate. A glass coverslip was then used to slowly drag the droplet from one end to the other end of the substrate. In this way, the (NH₄)₂MoS₄@GONSs were formed on the OTS-SiO₂/Si substrate. The MoS₂@RGO nanoscrolls (MoS₂@RGONSs) were prepared as shown in Scheme 1c,d. After the (NH₄)₂MoS₄@GONSs were put into a tube furnace, a mixture gas of N₂/H₂ (80/40 sccm) was introduced as a protective gas. Then, the temperature of the furnace increased to 400 °C gradually, with a speed of 10 °C/min, and was kept for 60 min. During

this period, $(\text{NH}_4)_2\text{MoS}_4$ was decomposed to MoS_2 , while GO was reduced to RGO at the same time. Therefore, the $\text{MoS}_2@\text{RGO}$ NSs were successfully obtained.



Scheme 1. Schematic diagram of the preparation of $(\text{NH}_4)_2\text{MoS}_4@\text{GO}$ and $\text{MoS}_2@\text{RGO}$ nanoscrolls. (a) A drop of $(\text{NH}_4)_2\text{MoS}_4$ and GO solution is dragged by the cover slip on the hydrophobic substrate. (b) The $(\text{NH}_4)_2\text{MoS}_4@\text{GO}$ nanoscroll is formed by molecular combing. (c) After the as-prepared $(\text{NH}_4)_2\text{MoS}_4@\text{GO}$ nanoscroll is treated at $400\text{ }^\circ\text{C}$ in the N_2/H_2 environment, $(\text{NH}_4)_2\text{MoS}_4$ is decomposed to MoS_2 nanosheets and GO is reduced to RGO. (d) The as-obtained $\text{MoS}_2@\text{RGO}$ nanoscroll after high temperature annealing. The inset in the top right shows the cross-section structure of the $\text{MoS}_2@\text{RGO}$ nanoscroll.

2.3. Characterizations

An optical microscope (ECLIPSE LV100ND, Nikon, Tokyo, Japan), AFM (Dimension ICON with Nanoscope V controller, Bruker, Billerica, MA, USA) and TEM (JEM-2100F JEOL, Tokyo, Japan) were used to characterize the as-prepared $(\text{NH}_4)_2\text{MoS}_4@\text{GONS}$ and $\text{MoS}_2@\text{RGONS}$. In addition, Raman spectroscopy and Raman mapping of the as-prepared $(\text{NH}_4)_2\text{MoS}_4@\text{GONS}$ and $\text{MoS}_2@\text{RGONS}$ were tested on a LabRAM HR Evolution Raman spectrometer (Horiba Jobin Yvon, Palaiseau, France) with a 532 nm laser focused through a $100\times$ objective lens.

2.4. Device Fabrication and Photodetection

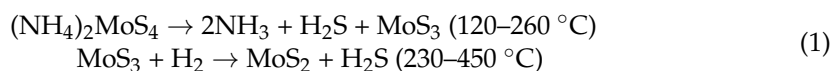
First, 30 nm thick gold and 5 nm thick chromium films were deposited on RGO and $\text{MoS}_2@\text{RGO}$ nanoscrolls, respectively, by thermal evaporation with a TEM grid (200 mesh) as a mask.

A probe station (model TTPX, Lake Shore Inc., Rhinelander, WI, USA) and Keithley 4200 semiconductor characterization system (Advanced Test Equipment Corp., San Diego, CA, USA) were used to monitor the real-time current change of the as-prepared devices. The photocurrent was collected from individual ROG and $\text{MoS}_2@\text{RGO}$ nanoscrolls with Au pads as the source and drain electrodes, respectively, as shown in Figure S1. The photo-detection test was recorded under blue (405 nm), green (532 nm) and red (633 nm)

lasers. The power of the laser was measured with a laser power meter (Laser power meter LP1, SanWa, Okayama, Japan).

3. Result and Discussion

Scheme 1 shows the preparation of MoS₂@RGONSs by molecular combing and thermal annealing. After the (NH₄)₂MoS₄ was wrapped into GO nanoscrolls by molecular combing, the (NH₄)₂MoS₄ was decomposed to MoS₂ at a high temperature under the atmosphere of N₂/H₂ [30]. It was found that the (NH₄)₂MoS₄ was decomposed to MoS₃ as the temperature increased from 120 to 260 °C under an inert atmosphere. The MoS₃ was further reduced to MoS₂ as the temperature was higher than 230 °C under N₂/H₂ [30]. The process can be described as the following chemical reactions,



We heated the (NH₄)₂MoS₄@GONSs in the temperature range of 300 to 500 °C. The Raman spectroscopy was used to characterize the amount of MoS₂ in GONSs by measuring the peak intensity of A_{1g}. As shown in Figure S2a, the peak intensity of A_{1g} increased as the temperature increased from 300 to 400 °C, while it decreased as the temperature further increased to 500 °C. The flow ratio of N₂ to H₂ also affects the formation of MoS₂ during the thermal annealing process. As shown in Figure S2b, the A_{1g} peak of the (NH₄)₂MoS₄@GONS annealed with a gas stream of 80 sccm N₂ and 40 sccm H₂ showed the highest intensity. Therefore, a mixture gas of N₂/H₂ (80/40 sccm) was introduced as a protective gas during the experiment. The concentration of the (NH₄)₂MoS₄ solution also has an important effect on the formation of (NH₄)₂MoS₄@GONSs and MoS₂@RGONSs. The peak intensity of A_{1g} increased as the concentration of (NH₄)₂MoS₄ solution increased from 5 mM to 30 mM, while it decreased when 50 mM (NH₄)₂MoS₄ solution was used (Figure S2c). In addition, the diameter of the (NH₄)₂MoS₄@GONSs increased as the concentration of (NH₄)₂MoS₄ increased from 5 mM to 50 mM (Figure S3). Meanwhile, the long and straight nanoscrolls were changed to irregular and thick aggregations. In order to wrap more MoS₂ and maintain the good scroll structure, (NH₄)₂MoS₄ solution with a concentration of 30 mM was used as the optimal concentration and annealed at 400 °C.

Figure 1a,b show the OM images of an (NH₄)₂MoS₄@GO nanoscroll before and after thermal annealing, respectively. It can be seen that the color of the nanoscroll changed from cyan to gray blue after thermal annealing. In addition, the height of the MoS₂@RGO nanoscroll is quite smaller than that of the (NH₄)₂MoS₄@GO nanoscrolls. As shown in Figure S4, the height of the (NH₄)₂MoS₄@GO is 201.4 nm, while it decreases largely to 112.5 nm after high temperature annealing, which could be attributed to the evaporation of water molecules trapped in the nanoscroll and the decomposition of (NH₄)₂MoS₄. In order to confirm the formation of the MoS₂@RGO nanoscroll, Raman spectroscopy was conducted at the same position of the nanoscroll before and after annealing. As shown in Figure 1c, there are only two Raman peaks located at 1359 and 1587 cm⁻¹ for the (NH₄)₂MoS₄@GO nanoscroll, which are assigned to the D and G peaks of GO. After thermal annealing, there are two more peaks located at 384.4 and 404.2 cm⁻¹ besides the D and G peaks, which are characteristics of MoS₂ nanosheets [31,32]. In addition, the intensity ratio of the D to G peak decreased from 1.24 to 0.72 for the (NH₄)₂MoS₄@GO nanoscroll after thermal annealing, indicating the formation of reduced GO (RGO). The D band originates from the lattice destruction of sp²-hybridized carbon, and the G band arises from the first-order scattering of the E_{2g}¹ mode. The intensity ratio (I_D/I_G) reflects the disorder of the carbon structure, and the higher intensity ratio of I_D/I_G means more defective graphitic structures. Therefore, the Raman characterization confirms the successful conversion of the (NH₄)₂MoS₄@GO nanoscroll to the MoS₂@RGO nanoscroll after thermal annealing at 400 °C for 60 min. In order to investigate whether the MoS₂ was uniformly wrapped into the RGO nanoscroll, the as-obtained MoS₂@RGO nanoscroll was characterized by Raman mapping. As shown in Figure 1d,e, the G peak of GO nanoscroll was unchanged after

thermal annealing. Meanwhile, the Raman mapping of the A_{1g} peak of MoS_2 showed a homogeneous signal (Figure 1f), indicating that the MoS_2 was uniformly distributed in the RGO nanoscroll.

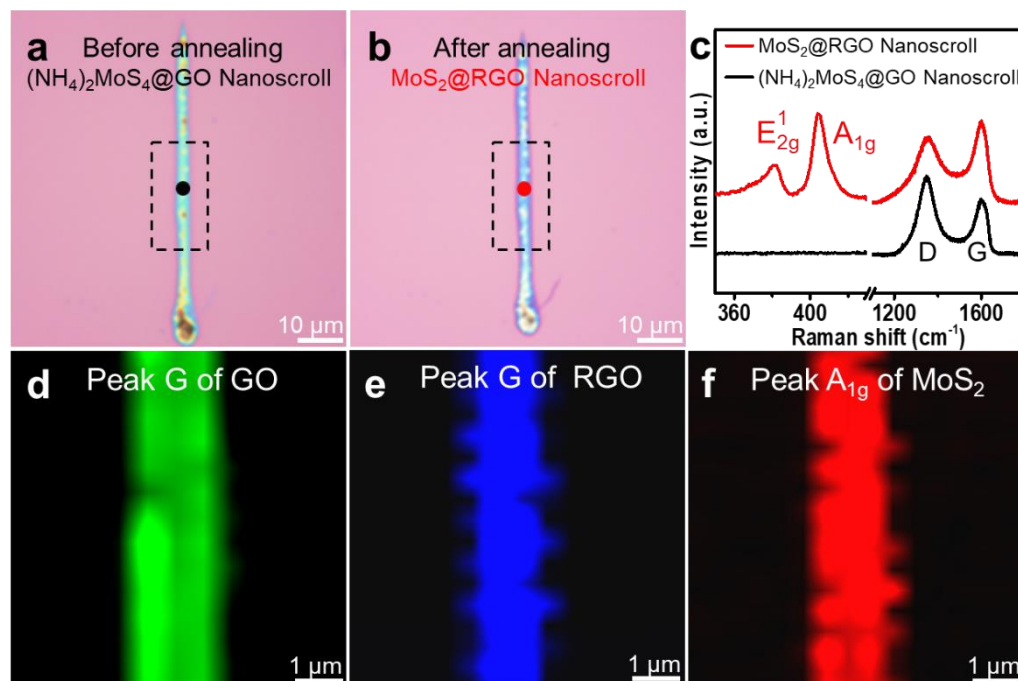


Figure 1. The OM images of the $(NH_4)_2MoS_4@GO$ nanoscroll (a) before and (b) after thermal annealing. (c) Raman spectra of the $(NH_4)_2MoS_4@GO$ and $MoS_2@RGO$ nanoscrolls. The Raman mapping images of (d) the $(NH_4)_2MoS_4@GO$ nanoscroll and (e) the RGO at peak G (1587 cm^{-1}), and the $MoS_2@RGO$ nanoscroll at peak (f) A_{1g} (404.2 cm^{-1}) of MoS_2 .

We found that the Raman peak intensity of MoS_2 in the $MoS_2@RGO$ nanoscrolls varied with the height of the nanoscrolls. To investigate the relationship between the height of the $MoS_2@RGO$ nanoscroll and the amount of trapped MoS_2 in it, the $MoS_2@RGO$ nanoscrolls with various heights were characterized using AFM and Raman spectroscopy, respectively. Figure 2a shows the OM image of the $MoS_2@RGO$ nanoscroll, where the boxes marked by d, e and f are three nanoscrolls with different heights. Figure 2d–f show the corresponding AFM images, and the measured heights of the three nanoscrolls are 137.4 nm, 83.5 nm and 35.4 nm, respectively. As shown in Figure 2b, the nanoscroll with a height of 137.4 nm presents a stronger Raman signal (box d), while the nanoscroll with a height of 35.4 nm has a weaker Raman signal. To further reveal the influence of the height of the $MoS_2@RGO$ nanoscrolls on the Raman peak intensity of MoS_2 , a lot of nanoscrolls were measured to plot the Raman peak intensity as a function of the height of the nanoscrolls. As shown in Figure 2c, with the increasing height of the $MoS_2@RGO$ nanoscrolls, the Raman peak intensity of MoS_2 gradually increases, indicating that more MoS_2 was trapped in a higher nanoscroll.

In order to clearly observe the detailed structure and confirm the formation of MoS_2 in the as-prepared $MoS_2@RGO$ nanoscroll, high-resolution transmission electron microscopy (HRTEM) was used for characterization. Figure 3a shows the low-resolution TEM image of the $MoS_2@RGO$ nanoscroll. We can see that the $MoS_2@RGO$ nanoscroll exhibits a multilayer scrolled structure with a dark, dense inner layer. Figure 3b shows the HRTEM characterization result of the red dashed box shown in Figure 3a. The well resolved lattice stripes with spacing of 0.63 nm are clearly presented, which is consistent with the interlayer spacing of layered MoS_2 [33]. Moreover, the energy dispersive X-ray (EDX) elemental mapping analysis of the $MoS_2@RGO$ nanoscroll shown in Figure 3c provides strong evidence for the homogeneous distribution of C, O, Mo and S elements in the

MoS₂@RGO nanoscroll. The HRTEM and EDX results confirm the uniform existence of the MoS₂ nanosheet in the RGO nanoscroll.

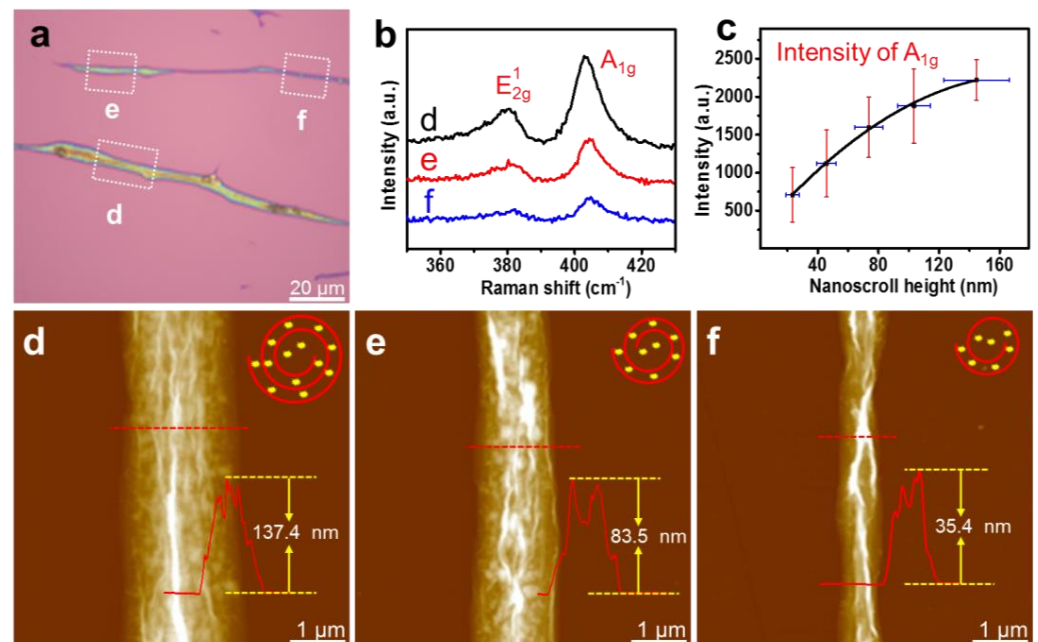


Figure 2. (a) The OM image of the MoS₂@RGO nanoscrolls. (b) The Raman spectra of MoS₂@RGO marked by dashed boxes of d, e and f shown in (a). (c) The plot of the Raman intensity of A_{1g} peak as a function of the height of the MoS₂@RGO nanoscrolls. (d–f) The corresponding AFM images of the MoS₂@RGO nanoscroll marked by dashed boxes of d, e and f shown in (a).

Graphene and its derivatives are severely limited in optoelectronic applications due to their zero band gap and poor absorption of visible light. In order to improve the optoelectronic performance of graphene, MoS₂, as a typical transition metal dichalcogenides (TMDCs) material, has been widely used to combine graphene for photodetection [34]. By wrapping MoS₂ into the RGO nanoscrolls, we found that the MoS₂@RGO nanoscroll also showed promising photodetection performance. Photodetectors based on RGO nanoscrolls and MoS₂@RGO nanoscrolls were fabricated to investigate the effect of wrapped MoS₂. It is well known that photosensitivity is an important parameter to evaluate the performance of photodetectors [35–37], which is usually defined by the ratio of photocurrent to dark current (PDR), as follows:

$$\text{PDR} = I_{\text{photo}}/I_{\text{dark}} \quad (I_{\text{photo}}: \text{photocurrent}; I_{\text{dark}}: \text{dark current}) \quad (2)$$

The photocurrent and dark current of the RGO nanoscrolls and MoS₂@RGO nanoscrolls-based photodetectors were firstly measured under the dark and the illumination of blue, red and green lasers with different laser power densities, respectively. Because of the low light absorption of RGO, we found that the RGO-based photodetectors exhibited photosensitivity of ~7, ~2.4 and ~4 under blue, red and green lasers (Figure S5). Figure 4a–c show the PDRs of photodetectors based on RGO nanoscrolls and MoS₂@RGO nanoscrolls under blue (405 nm), red (633 nm) and green (532 nm) lasers. The PDRs of photodetectors based on the MoS₂@RGO nanoscrolls were 570, 360 and 140 under blue, red and green lasers, which are almost 81, 144 and 35 times those of the photodetectors based on the RGO nanoscrolls measured under the same conditions. In addition, the photocurrent of the MoS₂@RGO nanoscroll is highly dependent on the power density of the incident light. As shown in Figure 4d–f, the PDRs increased as the incident laser power density increased. The different photoresponse of MoS₂@RGONS to blue, green and red light could be explained as follows. In our experiment, the power intensity of green light is the lowest.

However, the PDR of MoS₂@RGONS is around 140 at a power density of 0.56 mW/mm² (Figure 4f), while the PDRs of MoS₂@RGONS are around 100 and 70 for blue and red lasers at power densities of 1.05 mW/mm² and 1.41 mW/mm² (Figure 4d,e), respectively. The MoS₂ nanosheets synthesized in GONS could be multilayer, which can be confirmed by the HRTEM images shown in Figure 3b. Therefore, the multilayer MoS₂ trapped into RGONS should be more suitable for detecting green lasers than blue and red lasers given that they are at the same power intensity. A similar phenomenon has also been reported in a multilayer MoS₂@glassy-graphene heterostructure [38]. In addition, the MoS₂@RGONS shows higher PDR under the blue laser than under the red laser at similar power intensities. This could be attributed to the higher photon energy of the blue laser compared to the red laser, which can generate more photoinduced carriers at the same power [39].

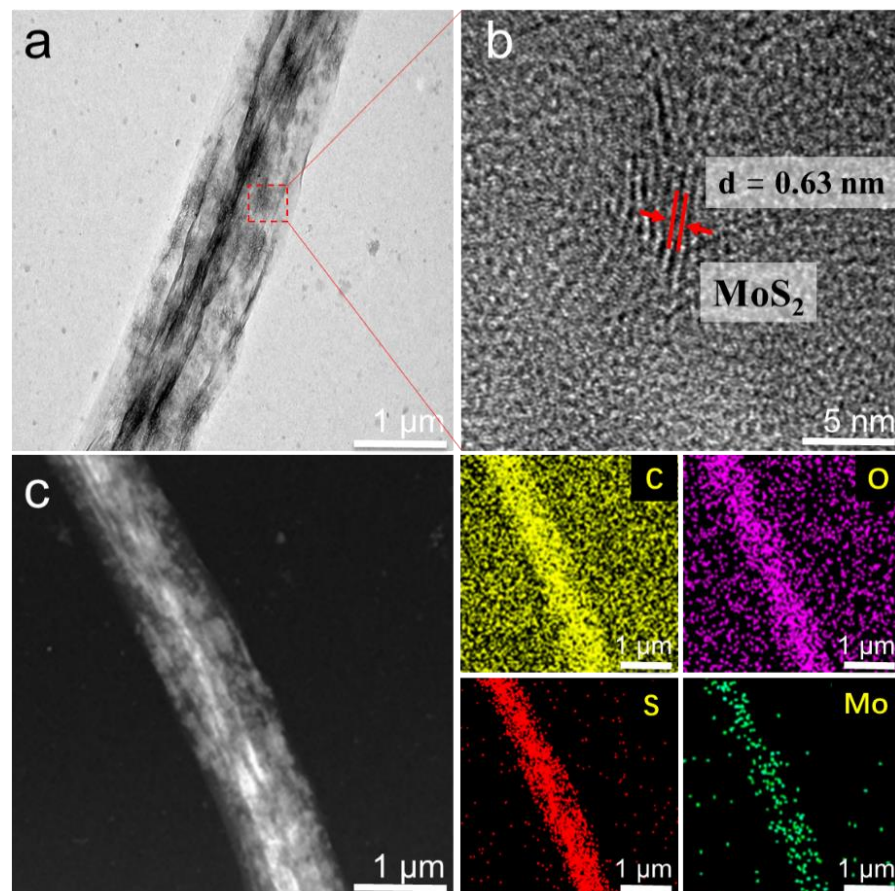


Figure 3. (a) The TEM image of the MoS₂@RGO nanoscroll. (b) HRTEM image of the MoS₂ nanosheets marked by the dashed box shown in (a). (c) The STEM image and EDX elemental mapping of the MoS₂@RGO nanoscroll.

The excellent photodetection performance of the MoS₂@RGO nanoscroll could be attributed to the formation of multiple heterojunction interfaces between the RGO and MoS₂ nanosheets. It is known that the ultrafast separation and transfer of photogenerated carriers can be achieved at the heterojunction interface of graphene and MoS₂, resulting in a substantial increase in photocurrent and photoresponse. Due to the roll-up structure of the MoS₂@RGO nanoscroll, the MoS₂ nanosheets are wrapped between adjacent RGO layers spirally, forming multiple heterojunction interfaces. When light was shined on the MoS₂@RGO nanoscroll, the MoS₂ nanosheets in each heterojunction interface could absorb light, and charge carriers were generated simultaneously. Meanwhile, the photo-generated charge carriers can be separated and transferred in an ultrafast way. Therefore, the photocurrent of the MoS₂@RGO nanoscroll can be greatly enhanced due to the syn-

ergetic enhancement of photocurrent at each heterojunction interface. As a consequence, the photosensitivity of the MoS₂@RGO nanoscroll is much higher than that of the RGO nanoscroll.

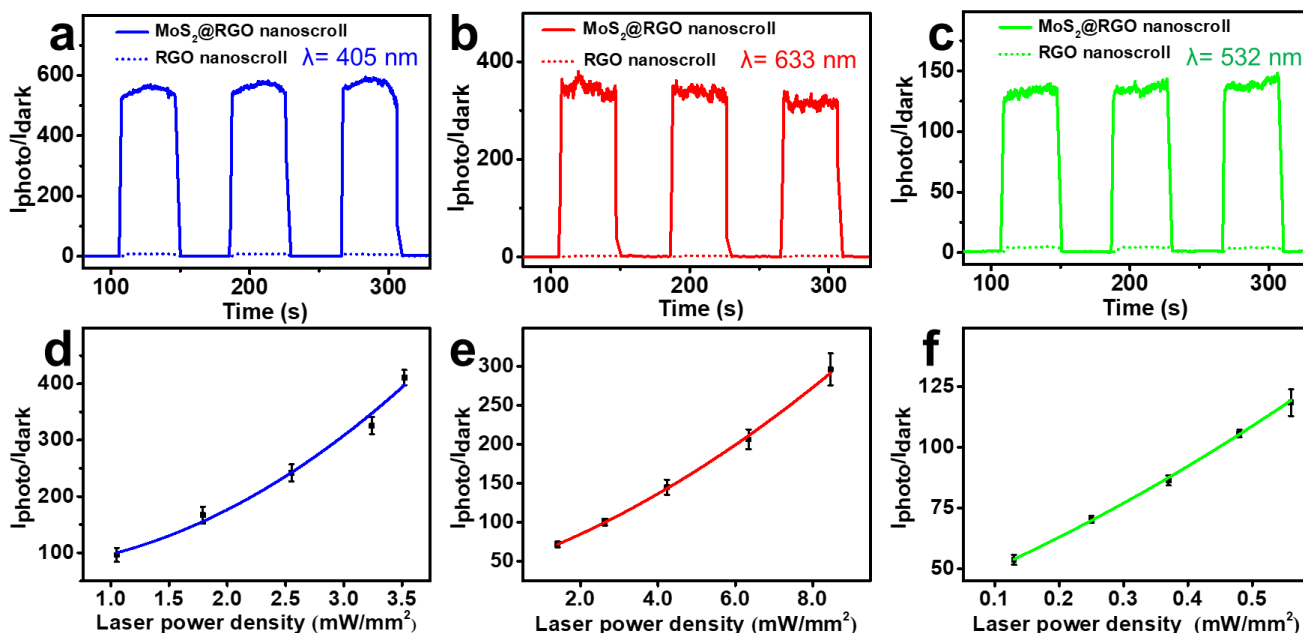


Figure 4. (a–c) The PDRs of photodetectors based on RGO and MoS₂@RGO nanoscrolls under (a) blue, (b) red and (c) green lasers. (d–f) Plots of PDR values of photodetectors based on MoS₂@RGO nanoscrolls under (d) blue, (e) red and (f) green lasers as a function of power density.

4. Conclusions

In summary, (NH₄)₂MoS₄ was encapsulated into the GO nanoscrolls by the molecular combing method on hydrophobic substrate. By optimizing the precursor concentration and annealing temperature, the (NH₄)₂MoS₄ and GO nanoscrolls were successfully converted to MoS₂ and RGO nanoscrolls, forming the MoS₂@RGO nanoscroll. The OM and AFM characterization results showed that the high-density MoS₂@RGO nanoscrolls were successfully prepared. The uniform distribution of the MoS₂ nanosheets in the RGO nanoscrolls was confirmed by the Raman spectroscopy and HRTEM characterization. Compared to the RGO nanoscroll, the MoS₂@RGO nanoscroll showed much better photodetection performance. The PDRs of photodetectors based on the MoS₂@RGO nanoscrolls were about two orders of magnitude higher than those of photodetectors based on the RGO nanoscrolls under blue, red and green lasers. The formation of multiple graphene/MoS₂ heterojunction interfaces in a scrolled structure can not only enhance the light absorption of MoS₂ but also accelerate the electron-hole separation. Our work indicates that the MoS₂@RGO nanoscrolls could be promising materials for high-performance graphene-based photodetectors.

Supplementary Materials: The following supporting information can be downloaded at <https://www.mdpi.com/article/10.3390/nano12091581/s1>: Figure S1. The optical images of photodetectors based on individual (a) RGO nanoscroll and (b) MoS₂@RGO nanoscroll with Au pads as source and drain electrodes. Figure S2. Plots of Raman peak intensity of A_{1g} as function of (a) annealing temperature, (b) the flow ratio of N₂ to H₂, and (c) concentration of (NH₄)₂MoS₄. Figure S3. OM images of (NH₄)₂MoS₄@GONS prepared by molecular combing (NH₄)₂MoS₄ solution with concentration of (a,e) 0.005 M, (b,f) 0.01 M, (c,g) 0.03 M, and (d,h) 0.05 M before and after thermal annealing. Figure S4. AFM height images of the same (NH₄)₂MoS₄@GONS (a) before and (b) after thermal annealing. Figure S5. PDR plots of RGO nanoscrolls measured under (a) blue, (b) red, and (c) green lasers.

Author Contributions: Conceptualization, H.L.; supervision and project administration, X.H. and H.L.; methodology, H.L. and X.L.; formal analysis, Z.W., F.L., X.L. and Y.Y.; investigation, Z.W. and X.L.; writing—original draft preparation, H.L., Z.W. and X.L.; revision of the manuscript, H.L. and Z.W. All authors have read and agreed to the published version of the manuscript.

Funding: This work was supported by the National Natural Science Foundation of China (Grant No. 51832001, 21571101 and 51322202), the Natural Science Foundation of Jiangsu Province in China (Grant No. BK20161543), and the Natural Science Foundation of the Jiangsu Higher Education Institutions of China (Grant No. 15KJB430016).

Institutional Review Board Statement: Not applicable.

Informed Consent Statement: Not applicable.

Data Availability Statement: Data can be available upon request from the authors.

Conflicts of Interest: The authors declare no conflict of interest.

References

1. Berman, D.; Deshmukh, S.A.; Sankaranarayanan, S.K.R.S.; Erdemir, A.; Sumant, A.V. Macroscale Superlubricity Enabled by Graphene Nanoscroll Formation. *Science* **2015**, *348*, 1118–1122. [[CrossRef](#)] [[PubMed](#)]
2. Chen, Z.; Wang, J.R.; Pan, D.X.; Wang, Y.; Noetzel, R.; Li, H.; Xie, P.; Pei, W.L.; Umar, A.; Jiang, L.; et al. Mimicking a Dog's Nose: Scrolling Graphene Nanosheets. *ACS Nano* **2018**, *12*, 2521–2530. [[CrossRef](#)] [[PubMed](#)]
3. Zhao, Y.; Wang, J.J.; Ma, C.L.; Cao, L.J.; Shao, Z.P. A Self-Adhesive Graphene Nanoscroll/Nanosheet Paper with Confined Fe_{1-x}S/Fe₃O₄ Hetero-Nanoparticles for High-Performance Anode Material of Flexible Li-Ion Batteries. *Chem. Eng. J.* **2019**, *370*, 536–546. [[CrossRef](#)]
4. Liu, P.W.; Jin, Z.; Katsukis, G.; Drahushuk, L.W.; Shimizu, S.; Shih, C.J.; Wetzel, E.D.; Taggart-Scarff, J.K.; Qing, B.; Van Vliet, K.J.; et al. Layered and Scrolled Nanocomposites with Aligned Semi-Infinite Graphene Inclusions at the Platelet Limit. *Science* **2016**, *353*, 364–367. [[CrossRef](#)] [[PubMed](#)]
5. Lai, Z.C.; Chen, Y.; Tan, C.L.; Zhang, X.; Zhang, H. Self-Assembly of Two-Dimensional Nanosheets into One-Dimensional Nanostructures. *Chem* **2016**, *1*, 59–77. [[CrossRef](#)]
6. Li, H.; Wu, J.; Qi, X.Y.; He, Q.Y.; Liusman, C.; Lu, G.; Zhou, X.Z.; Zhang, H. Graphene Oxide Scrolls on Hydrophobic Substrates Fabricated by Molecular Combing and Their Application in Gas Sensing. *Small* **2013**, *9*, 382–386. [[CrossRef](#)]
7. Wu, J.M.T.; Li, H.; Qi, X.Y.; He, Q.Y.; Xu, B.X.; Zhang, H. Graphene Oxide Architectures Prepared by Molecular Combing on Hydrophilic-Hydrophobic Micropatterns. *Small* **2014**, *10*, 2239–2244. [[CrossRef](#)]
8. Wu, J.; Yang, J.; Huang, Y.; Li, H.; Fan, Z.X.; Liu, J.Q.; Cao, X.H.; Huang, X.; Huang, W.; Zhang, H. Graphene Oxide Scroll Meshes Prepared by Molecular Combing for Transparent and Flexible Electrodes. *Adv. Mater. Technol.* **2017**, *2*, 1600231. [[CrossRef](#)]
9. Wang, L.; Yang, P.; Liu, Y.; Fang, X.R.; Shi, X.T.; Wu, S.Y.; Huang, L.; Li, H.; Huang, X.; Huang, W. Scrolling up Graphene Oxide Nanosheets Assisted by Self-Assembled Monolayers of Alkanethiols. *Nanoscale* **2017**, *9*, 9997–10001. [[CrossRef](#)]
10. Liu, Y.; Wang, L.; Zhang, H.; Ran, F.R.; Yang, P.; Li, H. Graphene Oxide Scroll Meshes Encapsulated Ag Nanoparticles for Humidity Sensing. *RSC Adv.* **2017**, *7*, 40119–40123. [[CrossRef](#)]
11. Zhao, W.H.; Wang, L.; Pei, C.J.; Wei, C.; You, H.; Zhang, J.D.; Li, H. Impact of pH on Regulating Ion Encapsulation of Graphene Oxide Nanoscroll for Pressure Sensing. *Nanomaterials* **2019**, *9*, 548. [[CrossRef](#)] [[PubMed](#)]
12. Tang, B.; Gao, E.L.; Xiong, Z.Y.; Dang, B.; Xu, Z.P.; Wang, X.G. Transition of Graphene Oxide from Nanomembrane to Nanoscroll Mediated by Organic Solvent in Dispersion. *Chem. Mater.* **2018**, *30*, 5951–5960. [[CrossRef](#)]
13. Fang, Q.L.; Zhou, X.F.; Deng, W.; Liu, Y.W.; Zheng, Z.; Liu, Z.P. Nitrogen-Doped Graphene Nanoscroll Foam with High Diffusion Rate and Binding Affinity for Removal of Organic Pollutants. *Small* **2017**, *13*, 201603779. [[CrossRef](#)] [[PubMed](#)]
14. Zheng, B.N.; Gao, C. Preparation of Graphene Nanoscroll/Polyaniline Composites and Their Use in High Performance Supercapacitors. *New Carbon Mater.* **2016**, *31*, 315–320. [[CrossRef](#)]
15. Rani, J.R.; Thangavel, R.; Oh, S.I.; Lee, Y.S.; Jang, J.H. An Ultra-High-Energy Density Supercapacitor: Fabrication Based on Thiol-functionalized Graphene Oxide Scrolls. *Nanomaterials* **2019**, *9*, 148. [[CrossRef](#)] [[PubMed](#)]
16. Li, X.J.; Natsuki, J.; Natsuki, T. A Recyclable Silver Nanoparticles/Graphene Oxide Nanoscroll Composite Photocatalyst. *Environ. Technol. Inno.* **2021**, *21*, 101210. [[CrossRef](#)]
17. Zhang, Y.F.; Zhao, C.Y.; Zeng, Z.H.; Ang, J.M.; Che, B.Y.; Wang, Z.; Lu, X.H. Graphene Nanoscroll/Nanosheet Aerogels with Confined SnS₂ Nanosheets: Simultaneous Wrapping and Bridging for High-Performance Lithium-Ion Battery Anodes. *Electrochim. Acta* **2018**, *278*, 156–164. [[CrossRef](#)]
18. Yang, B.J.; Chen, J.T.; Liu, B.; Ding, Y.X.; Tang, Y.; Yan, X.B. One Dimensional Graphene Nanoscroll-Wrapped MnO Nanoparticles for High-Performance Lithium Ion Hybrid Capacitors. *J. Mater. Chem. A* **2021**, *9*, 6352–6360. [[CrossRef](#)]
19. Lin, Y.T.; Zhou, F.S.; Chen, M.; Zhang, S.; Deng, C. Building Defect-Rich Oxide Nanowires@Graphene Coaxial Scrolls to Boost High-Rate Capability, Cycling Durability and Energy Density for Flexible Zn-Ion Batteries. *Chem. Eng. J.* **2020**, *396*, 125259. [[CrossRef](#)]

20. Cho, S.H.; Kim, J.H.; Kim, I.G.; Park, J.H.; Jung, J.W.; Kim, H.S.; Kim, I.D. Reduced Graphene-Oxide-Encapsulated MoS₂/Carbon Nanofiber Composite Electrode for High-Performance Na-Ion Batteries. *Nanomaterials* **2021**, *11*, 2691. [[CrossRef](#)]
21. Yoo, S.; Lee, J.; Kim, J.M.; Seong, C.Y.; Seong, K.D.; Piao, Y. Well-Dispersed Sulfur Wrapped in Reduced Graphene Oxide Nanoscroll as Cathode Material for Lithium-Sulfur Battery. *J. Electroanal. Chem.* **2016**, *780*, 19–25. [[CrossRef](#)]
22. Guo, Y.; Zhao, G.; Wu, N.T.; Zhang, Y.; Xiang, M.W.; Wang, B.; Liu, H.; Wu, H. Efficient Synthesis of Graphene Nanoscrolls for Fabricating Sulfur-Loaded Cathode and Flexible Hybrid Interlayer toward High-Performance Li-S Batteries. *ACS Appl. Mater. Inter.* **2016**, *8*, 34185–34193. [[CrossRef](#)] [[PubMed](#)]
23. Rani, J.R.; Thangavel, R.; Oh, S.I.; Woo, J.M.; Das, N.C.; Kim, S.Y.; Lee, Y.S.; Jang, J.H. High Volumetric Energy Density Hybrid Supercapacitors Based on Reduced Graphene Oxide Scrolls. *ACS Appl. Mater. Inter.* **2017**, *9*, 22398–22407. [[CrossRef](#)] [[PubMed](#)]
24. Liu, C.H.; Chang, Y.C.; Norris, T.B.; Zhong, Z.H. Graphene Photodetectors with Ultra-Broadband and High Responsivity at Room Temperature. *Nat. Nanotechnol.* **2014**, *9*, 273–278. [[CrossRef](#)] [[PubMed](#)]
25. Fan, H.C.; Wang, J.; Li, X.Y.; You, H.; Li, X.Z.; Pei, C.J.; Huang, X.; Li, H. Direct CVD Growth of MoS₂ on Chemically and Thermally Reduced Graphene Oxide Nanosheets for Improved Photoresponse. *APL Mater.* **2021**, *9*, 051105. [[CrossRef](#)]
26. Zhang, W.J.; Chuu, C.P.; Huang, J.K.; Chen, C.H.; Tsai, M.L.; Chang, Y.H.; Liang, C.T.; Chen, Y.Z.; Chueh, Y.L.; He, J.H.; et al. Ultrahigh-Gain Photodetectors Based on Atomically Thin Graphene-MoS₂ Heterostructures. *Sci. Rep.* **2014**, *4*, 3826. [[CrossRef](#)]
27. Gao, S.; Wang, Z.Q.; Wang, H.D.; Meng, F.X.; Wang, P.F.; Chen, S.; Zeng, Y.H.; Zhao, J.L.; Hu, H.G.; Cao, R.; et al. Graphene/MoS₂/Graphene Vertical Heterostructure-Based Broadband Photodetector with High Performance. *Adv. Mater. Interfaces* **2021**, *8*, 2001730. [[CrossRef](#)]
28. Rohizat, N.S.; Ripain, A.H.A.; Lim, C.S.; Tan, C.L.; Zakaria, R. Plasmon-Enhanced Reduced Graphene Oxide Photodetector with Monometallic of Au and Ag Nanoparticles at VIS-NIR Region. *Sci. Rep.* **2021**, *11*, 19688. [[CrossRef](#)]
29. Liu, Y.; Cheng, R.; Liao, L.; Zhou, H.L.; Bai, J.W.; Liu, G.; Liu, L.X.; Huang, Y.; Duan, X.F. Plasmon Resonance Enhanced Multicolour Photodetection by Graphene. *Nat. Commun.* **2011**, *2*, 579. [[CrossRef](#)]
30. Brito, J.L.; Ilija, M.; Hernandez, P. Thermal and Reductive Decomposition of Ammonium Thiomolybdates. *Thermochim. Acta* **1995**, *256*, 325–338. [[CrossRef](#)]
31. Mao, Y.; Dong, N.N.; Wang, L.; Chen, X.; Wang, H.Q.; Wang, Z.X.; Kislyakov, I.M.; Wang, J. Machine Learning Analysis of Raman Spectra of MoS₂. *Nanomaterials* **2020**, *10*, 2223. [[CrossRef](#)]
32. Lai, Y.Y.; Yeh, Y.W.; Tzou, A.J.; Chen, Y.Y.; Wu, Y.S.; Cheng, Y.J.; Kuo, H.C. Dependence of Photoresponsivity and On/Off Ratio on Quantum Dot Density in Quantum Dot Sensitized MoS₂ Photodetector. *Nanomaterials* **2020**, *10*, 1828. [[CrossRef](#)]
33. Fang, X.R.; Wei, P.; Wang, L.; Wang, X.S.; Chen, B.; He, Q.Y.; Yue, Q.Y.; Zhang, J.D.; Zhao, W.; Wang, J.L.; et al. Transforming Monolayer Transition-Metal Dichalcogenide Nanosheets into One-Dimensional Nanoscrolls with High Photosensitivity. *ACS Appl. Mater. Inter.* **2018**, *10*, 13011–13018. [[CrossRef](#)]
34. Seo, D.B.; Trung, T.N.; Bae, S.S.; Kim, E.T. Improved Photoelectrochemical Performance of MoS₂ through Morphology-Controlled Chemical Vapor Deposition Growth on Graphene. *Nanomaterials* **2021**, *11*, 1585. [[CrossRef](#)]
35. Wang, L.; Yue, Q.Y.; Pei, C.J.; Fan, H.C.; Dai, J.; Huang, X.; Li, H.; Huang, W. Scrolling Bilayer WS₂/MoS₂ Heterostructures for High-Performance Photo-Detection. *Nano Res.* **2020**, *13*, 959–966. [[CrossRef](#)]
36. Yue, Q.Y.; Wang, L.; Fan, H.C.; Zhao, Y.; Wei, C.; Pei, C.J.; Song, Q.S.; Huang, X.; Li, H. Wrapping Plasmonic Silver Nanoparticles inside One-Dimensional Nanoscrolls of Transition-Metal Dichalcogenides for Enhanced Photoresponse. *Inorg. Chem.* **2021**, *60*, 4226–4235. [[CrossRef](#)]
37. Zhao, Y.; You, H.; Li, X.Z.; Pei, C.J.; Huang, X.; Li, H. Solvent-Free Preparation of Closely Packed MoS₂ Nanoscrolls for Improved Photosensitivity. *ACS Appl. Mater. Inter.* **2022**, *14*, 9515–9524. [[CrossRef](#)]
38. Xu, H.; Han, X.Y.; Dai, X.; Liu, W.; Wu, J.; Zhu, J.T.; Kim, D.Y.; Zou, G.F.; Sablon, K.A.; Sergeev, A.; et al. High Detectivity and Transparent Few-Layer MoS₂/Glassy-Graphene Heterostructure Photodetectors. *Adv. Mater.* **2018**, *30*, 1706561. [[CrossRef](#)]
39. Naqi, M.; Kaniselvan, M.; Choo, S.; Han, G.; Kang, S.; Kim, E.; Yoon, Y.; Kim, S. Ultrasensitive Multilayer MoS₂-Based Photodetector with Permanently Grounded Gate Effect. *Adv. Electron. Mater.* **2020**, *6*, 1901256. [[CrossRef](#)]